IEEE Access
Multidisciplinary | Rapid Review | Open Access Journal

Date of publication xxxx 00, 0000, date of current version xxxx 00, 0000.

Digital Object Identifier 10.1109/ACCESS.2017.DOI

Contact Information-based Indoor Pedestrian Localization using Bluetooth Low Energy Beacons

SHINO SHIRAKI, (Member, IEEE), and SHIGEO SHIODA,(Member, IEEE)
Graduate School of Engineering, Chiba University, Chiba 263-8522, Japan

Corresponding author: Shino Shiraki (e-mail: s.shiraki@chiba-u.jp).

This work was supported by the Japan Society for the Promotion of Science KAKENHI Grant Number JP19H0213, JP22H01480, A-STEP, and JST SPRING Grant Number JPMJSP2109.

ABSTRACT Indoor localization technologies are actively investigated to realize location-based applications in various environments, and indoor localization methods based on whether the received signal strength indicator (RSSI) is less than a threshold have been proposed previously. Such a proximity/non-proximity binary value is used in digital contact tracing applications to reduce the coronavirus disease effects. We proposed two indoor pedestrian localization methods based on contact information using bluetooth low energy (BLE) beacons, namely multilateration and cooperative localization. This study attempts to demonstrate the effectiveness of the proposed methods using only contact information. Through simulation experiments, we found that the proposed methods can achieve comparable accuracy to existing methods when the attenuation model is accurate. The difference in average localization error was 0.1 m between the proposed method 1 and range-based method, and 0.2 m between the proposed method 2 and fingerprinting method. We confirmed that the proposed methods using only contact information are robust against environmental changes even when the attenuation model is inaccurate. We consider that these contributions have added a new perspective on the use of contact information in the field of indoor localization, which aims to realize power-saving and cost reduction.

INDEX TERMS Contact information, Indoor positioning, Nonlinear optimization, Proximity

I. INTRODUCTION

INDOOR localization has attracted increasing interest from industry to realize location-based applications in different environments. Recently, many studies have investigated indoor localization using BLE beacons [1]. Among these studies, a range-based method using trilateration or multilateration based on distances estimated from the RSSI of several BLE beacons is widely used. In addition, indoor localization based on "whether RSSI measurement is lower than the threshold P_{th}" rather than just the RSSI value has been studied [2]–[5]. In this method, the proximity relation between nodes is expressed by a binary value representing proximity or non-proximity.

$$\text{proximity} = \begin{cases} 0, & \text{RSS} \leq P_{th}, \\ 1, & \text{RSS} > P_{th}. \end{cases} \tag{1}$$

This proximity/non-proximity binary value is also used in digital contact tracing smartphone applications to reduce the effects of the coronavirus disease (COVID-19) pandemic. These smartphone applications notify the user of contact history with registered infected individuals using wireless communication technologies, e.g., such as Bluetooth and BLE [6]. In addition, digital contact tracing has been studied extensively [7], [8]. Contact information expressed as proximity or non-proximity is suitable for smartphones; thus, we consider that contact information between smartphones can be used for indoor pedestrian localization.

In a previous study, we proposed two indoor pedestrian localization methods based on contact information using BLE beacons [9]. The first method is multilateration and the second one is cooperative localization, which is an improved version of the sensor response-based localization technique [10], [11] for wireless sensor networks (WSNs). The sensor response-based localization technique uses proximity relations between nodes recognized from sensor responses to estimate the sensor position. Accordingly, this

study attempts to demonstrate the effectiveness of the proposed methods, which only use contact information.

BLE-based indoor localization methods can be classified into four types: range-based, fingerprinting, closest-beacon, and proximity methods. The accuracy of range-based methods, which use distances estimated directly from RSSI, would particularly deteriorate when the attenuation model used to calculate the distance between a pedestrian and a BLE beacon is inaccurate due to environmental changes. The proposed methods do not require a specific attenuation model. In fingerprinting methods, accurately estimating a position when the environment changes from the one where the RSSI map was measured in advance is difficult. However, the proposed methods have the advantage of being robust against environmental changes. Closest-beacon methods, which use the strongest beacon signal, require numerous BLE beacons for accurate localization, whereas the proposed methods require fewer BLE beacons. Further, the existing proximity-based methods focus on the one-hop proximity between a BLE beacon and a smartphone. Meanwhile, the proposed methods use the number of hops obtained from the proximity relation between smartphones for localization. The major contributions of this study are summarized as follows.

- We confirmed that the sensor response-based localization method [10], [11] for WSNs could be applied to indoor localization.
- Through simulation experiments, we found that the proposed methods could obtain comparable accuracy to existing methods when the attenuation model is accurate.
- We confirmed that the proposed methods were robust against environmental changes even when the attenuation model is inaccurate.

The remainder of this paper is organized as follows. Section II overviews previous studies on BLE-based indoor localization and other related works. Section III outlines the target problem and the proposed localization methods, and Section IV describes experiments conducted using real devices. In Section V, we discuss the effectiveness of the proposed methods through simulation experiments. Finally, conclusions are presented in Section VI.

II. RELATED WORK

Technologies that can be implemented on smartphones for indoor localization include radio frequency, self-contained sensors, indoor maps, and magnetic field fingerprinting [12]. Among these technologies, smartphone-based indoor positioning systems using radio frequency have been widely studied [13].

BLE was released in June 2010 as Bluetooth version 4.0. The features of BLE are short-range wireless communication and low power consumption. These features are suitable for mobile devices, e.g., smartphones and tablets, which are rapidly becoming ubiquitous. Thus, BLE is used for COVID-19 digital contact tracing applications, and in recent years, many studies have investigated indoor localization methods using BLE beacons.

As mentioned in Section I, BLE-based indoor localization methods can be classified into four types, and many methods that combine these techniques have been studied. The range-based method estimates the position by trilateration or multilateration based on the distances calculated from the RSSI value of BLE beacons. In recent years, the range-based method has been used for indoor positioning using BLE beacons in a smart museum [14]. However, the localization accuracy of the range-based method using RSSI is largely dependent on the radio propagation environment. Thus, methods to suppress the influence of RSSI fluctuations have also been studied [15]–[17]. The RSSI of the BLE measured by three frequency channels is different, and the attenuation model is different depending on the channel. To improve the adaptability and robustness of the BLE positioning system, Huang *et al*. proposed an indoor positioning method using the information of three BLE advertising channels [17]. Despite the above studies, the problem of the range-based methods associated with an attenuation model has not been completely solved. The proposed methods do not have such a problem because the methods do not require a specific attenuation model for localization.

The fingerprinting method determines the best matching coordinates by comparing RSSI measurements with a pre-measured RSSI map. A previous study [18] investigated the key parameters required to realize accurate indoor positioning using BLE radio signals. Another study [19] proposed a fingerprinting algorithm based on the general and weighted k-nearest neighbor algorithms. The fingerprinting method is expected to be used in a BLE-based indoor positioning system developed for monitoring the daily living patterns of the elderly or disabled [20]. In the fingerprinting method, it is difficult to estimate a position accurately when the environment changes from the one where the RSSI map was measured in advance. By contrast, the proposed methods have the advantage of being robust to environmental changes.

The closest-beacon method identifies the strongest signal received by the pedestrian and estimates the position of the source of that signal as the pedestrian's probable position. For example, Apple's iBeacon protocol [21] is a BLE-based short-range wireless communication technology designed for proximity detection and proximity-based service. The closest-beacon method has been widely studied [22]–[25], including zone-level occupancy detection [26]. Instead of identifying the strongest signal source, a method has been proposed to identify the source of the signal received by the pedestrian most times and estimate the position of that source as the pedestrian's probable position [27]. Although the closest-beacon method is simple and easily feasible, it requires numerous BLE beacons for accurate localization, whereas the proposed methods require fewer BLE beacons because the number of hops obtained from the proximity relation between smartphones is used for localization.

As well as our proposed methods, several existing studies have proposed proximity-based localization methods based on positional relationships with beacons represented by the

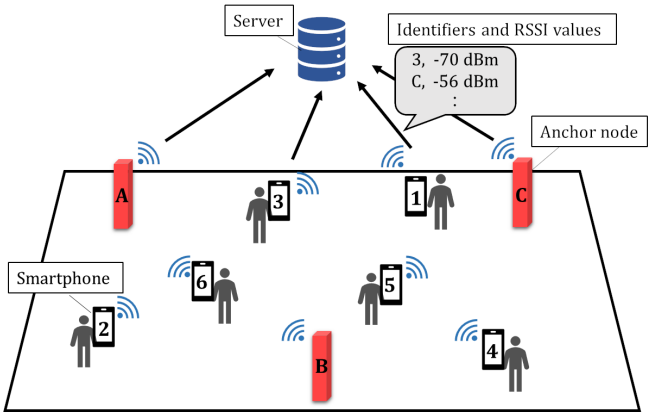

FIGURE 1. Problem settings.

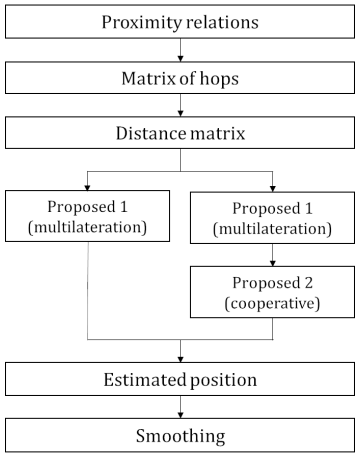

FIGURE 2. Overview of proposed methods.

binary value of proximity/non-proximity. In these studies, the proximity relation is determined by whether the RSSI measurement is less than a given threshold. For example, Fazio *et al*. proposed a proximity-based navigation system using BLE in a smart building [2], and Zhao *et al*. developed an RSS-proximity report-based particle filtering algorithm [3]. In addition, RSS threshold optimization techniques using a Gaussian process [4] and theoretical bounds for proximity report-based indoor positioning have been proposed [5]. These methods focus on the one-hop proximity between a BLE beacon and a smartphone. Meanwhile, the proposed methods use the number of hops obtained from the proximity relation between smartphones for localization.

Similar to our proposed methods, connectivity-based localization is being studied in the field of WSNs [28], [29]. This method defines two sensors that receive wireless signals as "proximity" and then localizes the sensors based on the connection relation expressed by the binary value. However, the application of this method to indoor pedestrian localization is limited; thus, it is unclear whether this method would be effective for indoor pedestrian localization because it is assumed that the sensor is fixed. The previously proposed sensor response-based localization technique [10], [11] is based on connectivity-based localization [28], [29] and cooperative localization [30], [31]. Furthermore, we have proposed two indoor pedestrian localization methods based on contact information using BLE beacons [9]. Note that our proposed methods target pedestrian localization rather than fixed sensor devices. The distance estimation method is similar to DV-HOP [32]; however, our methods are characterized by solving a mathematically backed nonlinear optimization problem.

III. PROBLEM SETTINGS AND CONTACT-BASED LOCALIZATION METHODS

A. PROBLEM SETTINGS

In this study, we consider pedestrian position estimation in a two-dimensional indoor area. The pedestrians in the area carry a smartphone that can transmit and receive BLE signals.

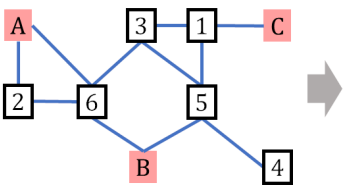

Matrix of hops

	1	2	3	4	5	6	A	B	C
1	0	3	1	2	1	2	3	2	1
2	3	0	2	4	3	1	1	2	4
3	1	2	0	2	1	1	2	2	2
4	2	4	2	0	1	3	4	2	3
5	1	3	1	1	0	2	3	1	2
6	2	1	1	3	2	0	1	1	3
A	3	1	2	4	3	1	0	2	4
B	2	2	2	2	1	1	2	0	3
C	1	4	2	3	2	3	4	3	0

FIGURE 3. Graph representing the proximity relation of nodes (left) and the matrix of hops (right).

In addition, several BLE beacons (i.e., anchor nodes) are placed at known positions. In the following, both the pedestrian's smartphone and the anchor nodes are referred to as nodes for simplicity. Each node periodically sends a wireless signal containing a list of identifiers and RSSI values of all nodes. Then, the server recognizes all node identifiers in the observation area and proximity relation. Here, if the RSSI value meets or exceeds a threshold, the server recognizes the proximity relation between the sender's listed nodes. Fig. 1 illustrates the problem settings.

We assume that the proximity relation between nodes is a binary value of 0 or 1. The proximity relation between nodes i and j at time t is expressed as follows.

$$\text{proximity}_{i,j}(t) = \begin{cases} 0, & \text{RSSI}_i \le R_{th} \text{ and } \text{RSSI}_j \le R_{th}, \\ 1, & \text{RSSI}_i > R_{th} \text{ or } \text{RSSI}_j > R_{th}, \end{cases} \tag{2}$$

where RSSI_i is the RSSI from node i, and R_{th} is the given RSSI threshold. Note that RSSI_i uses the aggregated RSSI rather than the channel separated RSSI. When $\text{proximity}_{i,j}(t) = 1$, nodes i and j are proximity, and when $\text{proximity}_{i,j}(t) = 0$, nodes i and j are non-proximity.

Then, the server expresses the proximity relation at each time as an undirected graph. The number of hops between the nodes in the undirected graph is then calculated by solving the shortest path problem. Fig. 2 shows an overview of the proposed methods, and Fig. 3 shows a graph representing the proximity relation of nodes and their matrix of hops. We then estimate the unknown position of the pedestrian.

B. ESTIMATING DISTANCE BETWEEN NODES BASED ON PROXIMITY RELATION

We calculate the average distance per hop and the distance between nodes from the proximity relation. Here, $\mathcal{N}$ is the set of pedestrian identifying numbers, and $\mathcal{A}$ represents the set of the anchor node identifying numbers. Let $\boldsymbol{a}_i$ denote the known coordinates of anchor node i. $\mathcal{P}_a$ gives the set of anchor node pairs that are connected in the undirected graph, and the number of hops between anchor nodes i and j ($(i,j) \in \mathcal{P}_a$) is denoted h_{ij}. The average distance per hop d_{avg} is calculated as follows.

$$d_{\text{avg}} = \frac{\sum_{(i,j)\in\mathcal{P}_a} |\boldsymbol{a}_i - \boldsymbol{a}_j|}{\sum_{(i,j)\in\mathcal{P}_a} h_{ij}}. \tag{3}$$

Then, we estimate the distance between nodes. Here, $\mathcal{P}$ denotes the set of node pairs connected in the undirected graph, and the number of hops between nodes i and j ($(i,j) \in \mathcal{P}$) is denoted h_{ij}. The matrix of hops is then multiplied by the average distance per hop d_{avg}, and the result is used for localization as a distance matrix $\{d_{ij}\}$. Using the average distance per hop d_{avg}, we calculate the distance between nodes d_{ij} as follows.

$$d_{ij} = d_{\text{avg}} h_{ij}. \tag{4}$$

C. PROPOSED METHOD 1: MULTILATERATION

We estimate the pedestrian's position from the distance between nodes d_{ij}. Proposed method 1 employs multilateration based on the distance between a pedestrian and three or more anchor nodes. In the following, the estimated coordinates of pedestrian $i(\in \mathcal{N})$ are represented by $\boldsymbol{r}_i$, which is expressed as follows.

$$\boldsymbol{r}_i = \arg\min_{\boldsymbol{x}} f(\boldsymbol{x}), \quad f(\boldsymbol{x}) \stackrel{\text{def}}{=} \sum_{j\in\mathcal{A}_i} (|\boldsymbol{x} - \boldsymbol{a}_j| - d_{ij})^2, \tag{5}$$

$$\mathcal{A}_i \stackrel{\text{def}}{=} \{j \in \mathcal{A}; (i,j) \in \mathcal{P}\}.$$

$\mathcal{A}_i$ is a set of anchor node identifying numbers connected to pedestrian i in the undirected graph. Equation (5) is used to find an estimated position that reproduces the distance between the pedestrian and the anchor nodes as accurately as possible.

The right-hand side of (5) is a nonlinear optimization problem; thus, it is difficult to find its optimal global solution. Therefore, we employ a numerical calculation method to obtain a local optimum solution. The initial solution is defined as follows.

$$\boldsymbol{r}_i^{(0)} = \frac{1}{|\mathcal{A}_i|} \sum_{j\in\mathcal{A}_i} \boldsymbol{a}_j. \tag{6}$$

The initial solution $\boldsymbol{r}_i^{(0)}$ is the centroid of the anchor nodes included in $\mathcal{A}_i$. Then, assuming that the $k-1$th solution is fixed, the kth solution can be obtained as follows.

$$\boldsymbol{r}_i^{(k)} = \frac{1}{|\mathcal{A}_i|} \sum_{j\in\mathcal{A}_i} \frac{d_{ij}(\boldsymbol{r}_i^{(k-1)} - \boldsymbol{r}_j)}{|\boldsymbol{r}_i^{(k-1)} - \boldsymbol{r}_j|} + \boldsymbol{r}_i^{(0)}. \tag{7}$$

Solutions $\boldsymbol{r}_i^{(1)}, \boldsymbol{r}_i^{(2)}, \ldots$ can be obtained recursively from the initial solution $\boldsymbol{r}_i^{(0)}$ using (7). Note that the kth solution $\boldsymbol{r}_i^{(k)}$ converges to the local minimum solution on the right-hand side of (5) at the limit of $k \to \infty$. This method is effective when $|\mathcal{A}_i| \geq 2$. When $|\mathcal{A}_i| = 0$, the center of the observation area is the estimated position, and when $|\mathcal{A}_i| = 1$, the position of the anchor node connected on the undirected graph is the estimated position.

D. PROPOSED METHOD 2: COOPERATIVE LOCALIZATION

In proposed method 1, the position of each pedestrian is estimated independently based on the distance between the pedestrian and the anchor nodes. Thus, proposed method 1 does not consider the distance between the pedestrians. In proposed method 2, which is an improved version of the sensor response-based localization method [10], [11] for WSNs, the distance between other pedestrians is considered, in addition to the distance between the pedestrian and anchor nodes. As a result, proposed method 2 improves the localization accuracy of proposed method 1.

First, we delete elements of the distance matrix $\{d_{ij}\}$ that correspond to the elements of three or more hops in the matrix of hops. If the distance between nodes i and j is deleted, it is assumed that node $i \notin \mathcal{N}_j$ and node $j \notin \mathcal{N}_i$. Here, $\mathcal{N}_i$ is a set of the pedestrian identifying numbers connected to pedestrian i in the undirected graph. As a result, proposed method 2 considers the distance of neighboring nodes within two or fewer hops. Here, we assume that each pedestrian is numbered from 1 to N ($N = |\mathcal{N}|$). In cooperative localization, we find the position of a pedestrian by solving the following optimization problem.

$$(\boldsymbol{r}_1, \ldots, \boldsymbol{r}_N) = \arg\min_{(\boldsymbol{x}_1,\ldots,\boldsymbol{x}_N)} g(\boldsymbol{x}_1, \ldots, \boldsymbol{x}_N), \tag{8}$$

where

$$g(\boldsymbol{x}_1, \ldots, \boldsymbol{x}_N) \stackrel{\text{def}}{=} \frac{1}{2} \sum_{i\in\mathcal{N}} \sum_{j\in\mathcal{N}_i} (|\boldsymbol{x}_i - \boldsymbol{x}_j| - d_{ij})^2 + \sum_{i\in\mathcal{N}} \sum_{j\in\mathcal{A}_i} (|\boldsymbol{x}_i - \boldsymbol{a}_j| - d_{ij})^2, \tag{9}$$

$$\mathcal{N}_i \stackrel{\text{def}}{=} \{j \in \mathcal{N}; (i,j) \in \mathcal{P}\}.$$

The estimated positions $(\boldsymbol{r}_1, \ldots, \boldsymbol{r}_N)$ are determined by minimizing the function $g(\boldsymbol{x}_1, \ldots, \boldsymbol{x}_N)$. We employ stress majorization [33], which is a descent method, to recursively find the solution. In addition, proposed method 2 uses the estimated position obtained by proposed method 1 as the initial solution because stress majorization requires an initial

TABLE 1. Main environment settings of Raspberry Pi.

Operating system	Raspbian	ver. 11 (bullseye)
Execution environment	Node.js	ver. 9.2.1
Library	npm	ver. 5.5.1
Library	bleacon	ver. 0.5.1
Library	date-utils	ver. 1.2.21
Library	csv-writer	ver. 1.6.0

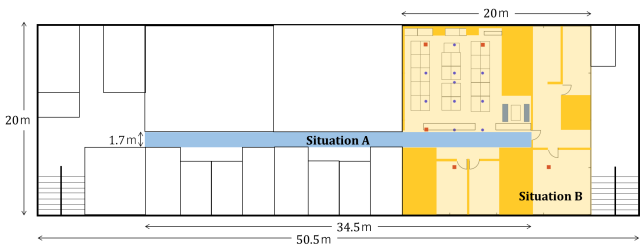

FIGURE 4. Overview of the laboratory floor.

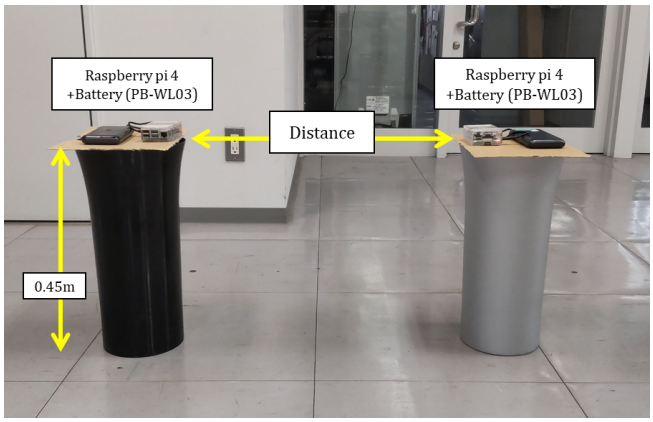

FIGURE 5. Preliminary experimental environment of situation A.

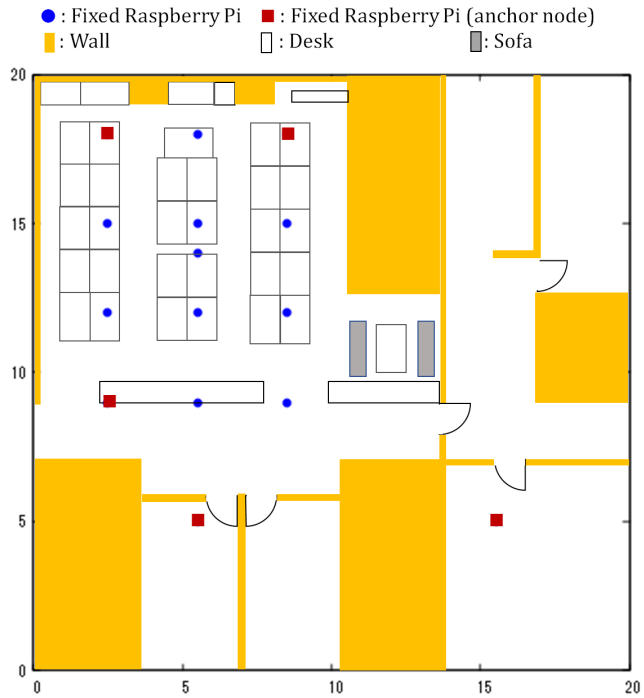

FIGURE 6. Preliminary experimental environment of situation B.

solution. Refer to the APPENDIX for details about how we formulate the optimization problem and its solution.

E. SMOOTHING

Finally, we employ the exponential smoothing technique to absorb the time variation of the estimated position of each node. The estimated position of node i at time t ($t = 1, 2, \dots$) is defined as $\boldsymbol{r}_i(t)$, and we calculate the estimated position after smoothing $\boldsymbol{r}_i^{\mathrm{smth}}(t)$ as follows.

$$\boldsymbol{r}_i^{\mathrm{smth}}(t) = \begin{cases} \boldsymbol{r}_i(t), & t = 1, \\ (1-\alpha)\boldsymbol{r}_i^{\mathrm{smth}}(t-1) + \alpha \boldsymbol{r}_i(t), & t = 2, 3, \dots, \end{cases} \tag{10}$$

where α is learning rate (here, $\alpha = 0.2$).

IV. EXPERIMENTAL EVALUATION

A. ATTENUATION MODEL

Here, we define an attenuation model from RSSI measurements taken in a real-world indoor environment to demonstrate that localization is possible using real devices. We adopted a commonly used log-distance path loss model. In this model, the relationship between RSSI (dBm) and distance (m) is expressed as follows.

$$\mathrm{RSSI}(d) = -10n \log_{10}\left(\frac{d}{d_0}\right) + \mathrm{RSSI}(d_0), \tag{11}$$

where $\mathrm{RSSI}(d)$ is the RSSI value at distance d, and $\mathrm{RSSI}(d_0)$ is the RSSI value at the reference distance d_0. n is the path loss exponent, which has a theoretical value of $n = 2$ in free space without obstacles. Note that obstacles, e.g., furniture and pedestrians, we present in indoor measurement environment, and the measured RSSI contained noise.

B. PRELIMINARY RSSI MEASUREMENT EXPERIMENTS

We conducted a preliminary RSSI measurement experiment on a laboratory floor. Fig. 4 shows an overview of the laboratory floor. Situation A was a corridor, and situation B was a laboratory area, including walls. Here, we used a Raspberry Pi 4 model B [34] to send and receive BLE signals. The Raspberry Pi was used in this preliminary experiment because it is inexpensive and easy to handle. In this experiment, the Raspberry Pi employed iBeacon [21] to send BLE signals at 100-ms intervals and received the signals from another Raspberry Pi. Then, the measured RSSI, received time, and sender identifier were recorded in an external CSV file. Table 1 shows the main environment settings of the Raspberry Pi.

We estimated the attenuation model parameters n and $\mathrm{RSSI}(d_0)$ from actual measurements using least squares estimation. The preliminary experimental environments for situ-

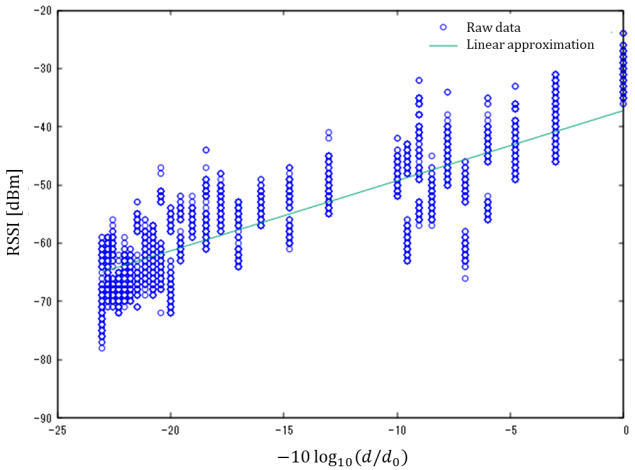

FIGURE 7. Parameter estimation results for situation A.

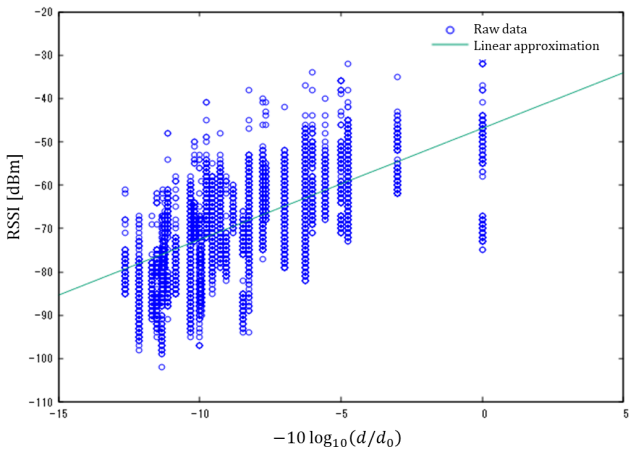

FIGURE 8. Parameter estimation results for situation B.

ations A and B are shown in Fig. 5 and Fig. 6, respectively. In situation A, RSSI measurements were collected when the distance between the two Raspberry Pi devices was varied from 0.1 to 20.0 m in the corridor environment. Then, parameter estimation was performed using 55,100 measurements from 29 unique distances. Here, the reference distance d_0 was set to 1.0 m. In situation B, we installed 15 Raspberry Pi devices on desks in the laboratory area and collected RSSI measurements. The laboratory area was surrounded by walls, and some desktop computers and furniture were present in the laboratory. Raspberry Pi devices at the lower left and right sides in Fig. 6 communicated through the wall with the door closed. We collected 62,000 measurements from 31 unique distances from 1.0 to 18.4 m, and estimated the parameters of the attenuation model. Here, the reference distance d_0 was set to 1.0 m. Fig. 7 and Fig. 8 shows the parameter estimation results for situation A and B, respectively.

According to the estimation results for situation A shown in Fig. 7, n = 1.21, RSSI(d_0) = −49.27 dBm, and the correlation coefficient between RSSI and distance between nodes was 0.85. In Fig. 8, which shows the estimation results for situation B, n = 2.56, RSSI(d_0) = −46.90 dBm, and the correlation coefficient between RSSI and distance between nodes was 0.72. These two situations are referred to as attenuation models A and B, respectively. The path loss exponent of the attenuation model B (n = 2.56) is much larger than that of the attenuation model A (n = 1.21). This result seems reasonable because there are some obstacles (like walls) in situation B, but no obstacles in situation A. Fig. 9 shows the attenuation models A and B.

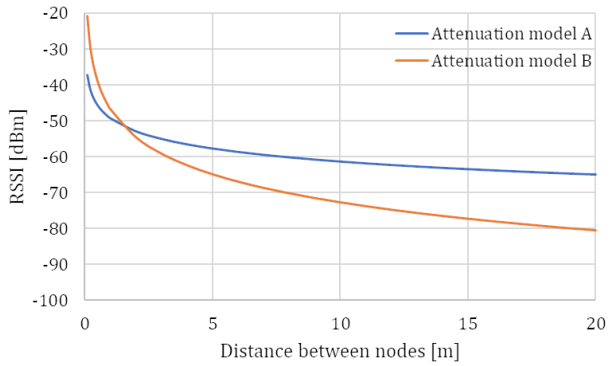

FIGURE 9. The attenuation models A and B.

As shown in Fig. 9, the RSSI attenuates as the distance between nodes increases. When the distance between the Raspberry Pi devices was greater than 7 m, the RSSI value obtained from the attenuation model A was in a narrow range, i.e., −60 to −65 dBm. When the distance is relatively long (>7 m), there will be a significant error in estimating the distance from the fluctuating RSSI measurement. At short distances (≤6 m), the RSSI was widely distributed from −37 to −60 dBm. Thus, if the distance between nodes is relatively short (e.g., 6 m), the proximity relation between nodes can be estimated correctly from the RSSI measurement and RSSI threshold. This is why we focused on indoor localization based on contact information (i.e., the proximity relation) between the nodes.

The attenuation models differ according to the surrounding, as shown by the attenuation models A and B. Note that the BLE signal is transmitted on one of three BLE advertising channels that use different frequencies. The attenuation models A and B are aggregated models of the three advertising channels, although the propagation characteristics of the advertising channels should be different. Three BLE advertising channel's information were used to develop three independent attenuation models for each BLE advertising channel in an indoor positioning approach proposed by Huang *et al.* [17]. However, a previous study [7] stated that a smartphone is typically not given access to information on which about the advertising channel from which a packet has been received. The attenuation model for each BLE

TABLE 2. Conditions of the attenuation model used in the real-world experiment and the simulations.

Result	Attenuation model used in existing methods	Actual radio propagation env.
Real-world laboratory env. (Fig. 10)	Model B (accurate) Model A (inaccurate)	Model B
Effect of RSSI threshold (Fig. 13)	Model A (accurate) Model B (inaccurate)	Model A
Dependence on # of anchors (Fig. 16)	Model A	Model A
Dependence on path loss exp. n (Fig. 17)	Model A	Model A (accurate) n=1.4-2.6 (inaccurate)

advertising channel was not established in this study since it was assumed that pedestrian's smartphones could not identify the BLE advertising channel. Note that our proposal can be extended to where pedestrian's smartphones can identify the advertising channel by setting different RSSI thresholds for each channel.

C. LOCALIZATION EXPERIMENT CONDITIONS

We also conducted a localization experiment using 15 fixed Raspberry Pi devices to confirm that localization is possible in a real-world environment. Here, the 15 Raspberry Pi devices were positioned on desks in the laboratory (Fig. 6). The five nodes represented by red squares in Fig. 6 are the anchor nodes. Note that the Raspberry Pi devices employed iBeacon to send BLE signals at 100-ms intervals and received the signals from the other Raspberry Pi. Then, the measured RSSI, received time, and sender identifier were recorded in an external CSV file. Here, the proximity relation was recognized from the given RSSI threshold R_{th}, RSSI_i and RSSI_j using (2). The average value of the RSSI measurements for 1 s was used the RSSI_i and RSSI_j for proximity recognition, and localization was performed at 1-s intervals.

In the proposed methods using the proximity relation, the recognized proximity relation depends on RSSI threshold R_{th}. For example, when R_{th} is high, the rate of proximity node pairs decreases, and when R_{th} is low, the rate of proximity node pairs increases. We evaluated the localization accuracy of the proposed methods by varying the value of RSSI threshold R_{th} from −50 to −70 dBm.

We compared the proposed methods with the *range-based* method, one of the well-known methods for localization. In the range-based method, a pedestrian's smartphone estimates its distance to the anchor nodes based on the strength of the signal transmitted by the anchor nodes and estimates the position using a multilateration technique. The distance between the pedestrian and the anchor node d is estimated by the following equation.

$$d = d_0 \times 10^{\left(\frac{\mathrm{RSSI}(d_0) - \overline{\mathrm{RSSI}}}{10n}\right)}. \tag{12}$$

where, $\overline{\mathrm{RSSI}}$ is the RSSI of the average strength of radio signals from the anchor node. For d_0, n, and $\mathrm{RSSI}(d_0)$, the parameters of the attenuation model A or B were used.

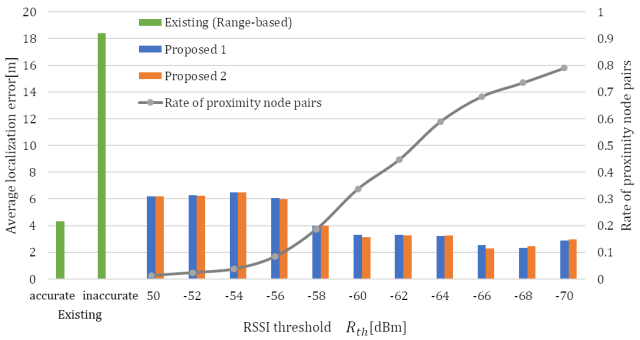

FIGURE 10. Results obtained in real-world laboratory environment.

We evaluated the accuracy of the localization methods at time t in terms of the *average localization error*, denoted by $\mathrm{err}(t)$, defined below.

$$\mathrm{err}(t) = \frac{1}{|\mathcal{N}|} \sum_{i \in \mathcal{N}} |\boldsymbol{r}_i^{\mathrm{smth}}(t) - \boldsymbol{r}_i^{\mathrm{actual}}(t)|. \tag{13}$$

Here, $\boldsymbol{r}_i^{\mathrm{actual}}(t)$ is the actual position of node i at time t. We compared the average localization error for 100 s in this localization experiment.

The characteristics of the area, such as the furniture arrangement and the population in the area, which frequently vary over time, have a substantial impact on the accuracy of the range-based method. The accuracy of the range-based method would particularly suffer when the attenuation model used to calculate the distance between the pedestrian and the anchor node was inaccurate. As described in Section IV-D, we evaluated the range-based method under two scenarios. The first scenario is where the attenuation model used for the distance estimation was accurate. In this scenario, the distance between the pedestrian and the anchor node was estimated by the attenuation model B. Note that the attenuation model B was identified in situation B (Fig. 8), where the experiment was conducted. In the second scenario, the attenuation model was inaccurate; the distance between the pedestrian and the anchor node was estimated by the attenuation model A. The simulation experiments in Section V also used these scenarios. Table 2 shows the conditions of the attenuation model used in the experiment and simulations.

D. RESULTS IN REAL-WORLD LABORATORY ENVIRONMENT

Fig. 10 shows the average localization errors of the proposed methods and the range-based method. In particular, the figure shows the average localization error of the proposed methods by changing the RSSI threshold R_{th} from −50 to −70 dBm. As shown in Fig. 10, when the attenuation model used in the range-based method is accurate, the localization accuracy of the range-based method and the proposed methods are similar. However, when the attenuation model is inaccurate,

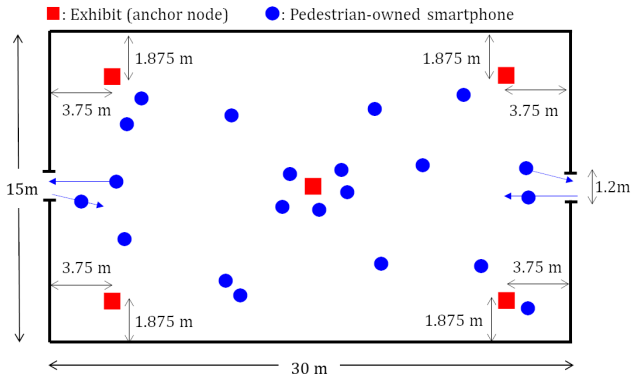

FIGURE 11. Indoor exhibition hall.

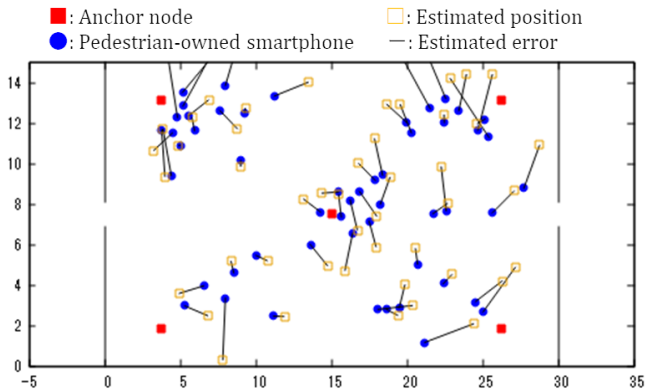

FIGURE 12. Example localization result obtained by proposed method 2. The average localization error was 1.2 m.

the localization accuracy of the range-based method is much worse than that of the proposed methods. Note that the proposed methods do not require a specific attenuation model.

Fig. 10 also shows that the localization accuracy of the proposed methods are fairly robust against the change in the RSSI threshold R_{th}. However, when R_{th} was set from −50 to −56 dBm, the rate of the proximity node pairs was 10% or less. With the proposed method 1, when $|\mathscr{A}_i| = 0$, the center of the observation area was the estimated position. Thus, with these threshold values, the estimated position was the center of the area, and the average localization error was approximately 6 m. When R_{th} was set from −58 to −70 dBm, the average localization error of the proposed methods was reduced to 2.3 m.

We confirmed that the sensor response-based localization method for WSNs could be applied to indoor localization in the real-world laboratory environment. However, Fig. 10 shows the result obtained using a small number of nodes. Accordingly, it is necessary to evaluate localization accuracy using a large number of nodes in a wide area to confirm the effect of the RSSI threshold.

V. SIMULATION EXPERIMENTS AND DISCUSSIONS

A. SIMULATION CONDITIONS

Here, through large-scale simulation experiments, we demonstrate that the proposed methods can obtain comparable accuracy to the existing methods. In addition, we confirmed that the proposed methods were robust against environmental changes even when the attenuation model is inaccurate.

In this evaluation, we considered a two-dimensional indoor exhibition hall with two doorways and five exhibits. Fig. 11 shows the indoor exhibition hall. Pedestrians with smartphones entered the observation area according to a Poisson process with an average arrival interval. The pedestrians visited the five exhibits in random order and viewed them for an average of 10 s according to an exponential distribution. Then, they exited through a doorway (different from the entrance). Here, the pedestrians moved according to the social force model [35], [36] via self-driving force and repulsive force from other pedestrians and walls. We set the maximum pedestrian speed to 0.25 m/s. In addition, a BLE beacon device was installed as an anchor node at each exhibit. We assumed that a pedestrian's smartphone and the anchor node can receive the signals transmitted by neighbor nodes.

In these simulation experiments, we assumed that the average strength of the radio signal from a pedestrian's smartphone or an anchor node at a distance of d is determined by (11). Note that radio signals in an actual environment are affected by fading. Here, we assumed that the received power distribution follows an exponential distribution via Rayleigh fading. The proximity relation between all pairs of nodes, where a node is a pedestrian or an anchor, is recognized in terms of (2) based on the strength of the radio signal exchanged between the two nodes. The pedestrian's positions were estimated at 1-s intervals based on the recognized proximity relations. In the simulation results shown below, the average localization error from 1000 to 1500 s from the start of the simulation was used. Fig. 12 shows an example localization result.

We compared the proposed methods with the fingerprinting and range-based methods. The fingerprinting method determines the best matching coordinates by compareing RSSI measurements with a premeasured RSSI map. The observation area is divided into grids of 0.5 m, and let $\boldsymbol{p}_i$ denote the coordinates of point i. First, a pedestrian at point i and the anchor node j are measured, and the average value of 1000 RSSI values between them is recorded as $\mathrm{RSSI}_j^{(i)}$. Then, $\boldsymbol{p}_i$ that minimizes the function m is calculated from the average value RSSI_j of 10 RSSI measurements between the pedestrian and anchor node j using the following equation.

$$\boldsymbol{p}_i = \arg\min_i m(i), \quad m(i) \stackrel{\text{def}}{=} \sum_{j \in \mathscr{A}} |\mathrm{RSSI}_j^{(i)} - \mathrm{RSSI}_j|. \quad (14)$$

B. EFFECT OF RSSI THRESHOLD

In the fingerprinting method, it is difficult to estimate the position accurately when the environment changes from the

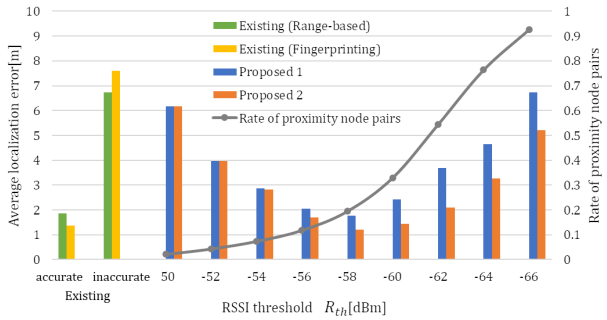

FIGURE 13. Comparison results of the RSSI threshold value effects.

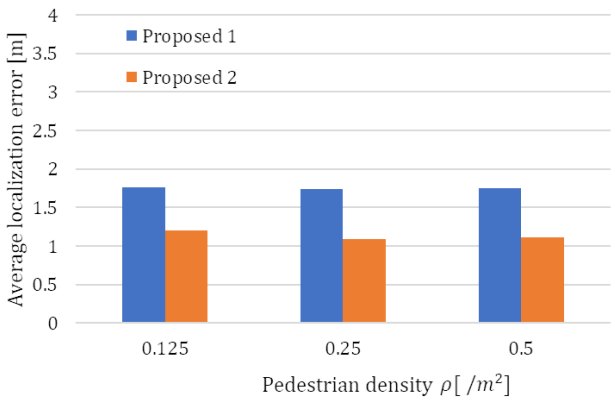

FIGURE 14. Comparison results of the pedestrian density effects.

one where the RSSI map was measured in advance. In other words, the attenuation model should be accurate for both the range-based and the fingerprinting methods.

We compared the proposed methods to the aforementioned two existing methods. The proposed methods do not require a specific attenuation model, and only the RSSI threshold must be determined appropriately. We assumed that the RSSI from pedestrian and anchor node at a distance of d is given by (11) with the parameter of attenuation model A (d_0 = 1.0 m, n = 1.21, RSSI(d_0) = −49.27 dBm). Here, a simple smoothing technique was applied to suppress RSSI fluctuation using the average value of 10 RSSI measurements. Here, the value of pedestrian density ρ was 0.125 $/m^2$, and the average arrival interval was 10 s. We evaluated the localization accuracy of the proposed methods by varying the RSSI threshold R_{th} from −50 to −66 dBm. Fig. 13 shows comparison results of the RSSI threshold value effects. The result obtained using the existing methods when the attenuation model is accurate or inaccurate are also shown for comparison. The attenuation model B was used for distance estimation and premeasured RSSI map generation when the attenuation model was assumed to be inaccurate. For path loss exponent dependencies, refer Section V-E for detailed results.

As shown in Fig. 13, the proposed methods with R_{th} set to −58 dBm can obtain comparable accuracy to the existing methods when the attenuation model is accurate. The difference in average localization error was 0.1 m between the proposed method 1 and range-based method, and 0.2 m between the proposed method 2 and fingerprinting method. On the other hand, the localization accuracy of the proposed methods outperform to existing methods when the attenuation model is inaccurate. Note that the proposed methods do not require a specific attenuation model; thus, the localization accuracy of the proposed methods does not depend on attenuation model. Furthermore, we found that localization accuracy was the best when the rate of the proximity node pairs was approximately 20%. In the following results, we set the RSSI threshold R_{th} such that the rate of proximity node pairs was 20%.

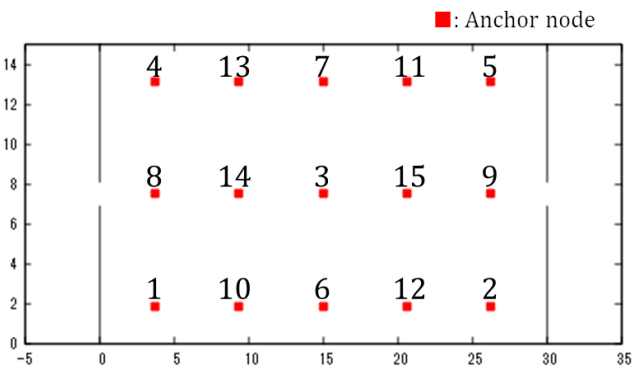

FIGURE 15. Identifiers of the anchor nodes and their positions.

C. EFFECT OF PEDESTRIAN DENSITY

We considered that the localization accuracy of the proposed methods is dependent on pedestrian density because the proximity relation depends on the number of pedestrians. Thus, we investigated the localization accuracy of the proposed methods for three pedestrian densities; 0.125 $/m^2$, 0.25 $/m^2$, and 0.5 $/m^2$; corresponding to the cases where the pedestrians arrived at the exhibition hall with average arrival intervals of 10 s, 6 s, and 4 s, respectively. Fig. 14 shows comparison results of the pedestrian density effects.

As shown in Fig. 14, there was almost no effect on the average localization error due to pedestrian density changes. The proposed method 1 uses RSSI measurements between the pedestrian and anchor nodes; thus, we considered that the pedestrian density had a minor effect on the localization accuracy. When the pedestrian density was increased from 0.125 $/m^2$ to 0.25 $/m^2$, the average localization error decreased by 0.1 m in the proposed method 2, which considered the distance between the pedestrians.

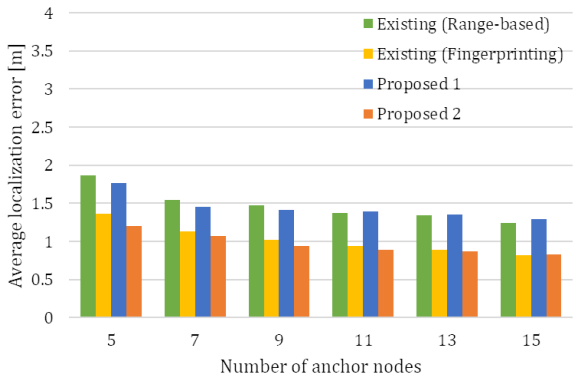

FIGURE 16. Comparison results of the number of anchor nodes effects obtained when the attenuation model is accurate.

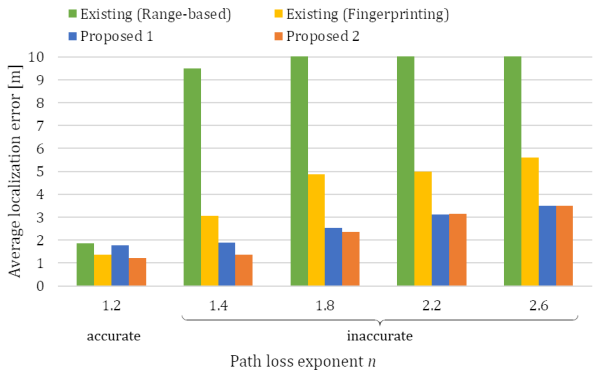

FIGURE 17. Comparison results of the path loss exponent value effects obtained when the attenuation model is inaccurate.

D. DEPENDENCE ON NUMBER OF ANCHOR NODES WHEN THE ATTENUATION MODEL IS ACCURATE

We considered that the localization accuracy also depends on the number of anchor nodes because the proposed methods estimate the distance from the proximity relation between the nodes. We investigated the effect of the number of the anchor nodes on localization error. Here, the pedestrian density ρ was 0.125 $/m^2$. The anchor nodes were given identifiers from 1 to 15. Fig. 15 shows the identifiers of the anchor nodes and their positions. We changed the number of the anchor nodes in order of the identifiers and compared the average localization errors. Fig. 16 shows comparison results of the number of anchor nodes effects obtained when the attenuation model is accurate.

As shown in Fig. 16, as the number of anchor nodes increases, the average localization error decreases for all methods. However, when the number of the anchor nodes is seven or greater, the error reduction range is only 0.2 to 0.3 m. Thus, we found that seven anchor nodes are sufficient to estimate the node positions under the conditions of this study. Note that using additional anchor nodes may effectively improve the localization accuracy when the attenuation model is inaccurate.

E. DEPENDENCE ON THE PATH LOSS EXPONENT OF THE ATTENUATION MODEL WHEN THE ATTENUATION MODEL IS INACCURATE

In Sections V-B to V-D, we assumed a case where the actual radio propagation environment is fixed and the advance assumed attenuation model is accurate and inaccurate when using the existing methods. However, when pedestrians use position estimation applications, environmental conditions, e.g., the furniture arrangement and the population in the area, often change over time. Here, we considered a case where the actual radio propagation environment is changed and the advance assumed attenuation model is fixed. In this evaluation, we considered a situation where the path loss exponent n is changed from 1.4 to 2.6 from the preset attenuation model A.

In the proposed methods, we used an RSSI threshold of −58 dBm, which is the rate of proximity node pairs of 20% assumed in Section V-B with the attenuation model A. In the fingerprinting method, we used the RSSI generated using the attenuation model A when the RSSI map was measured in advance. The proposed methods were compared with the existing methods. Fig. 17 shows comparison results of the path loss exponent values when the attenuation model is inaccurate.

As shown in Fig. 17, the average localization error increases with the increasing path loss exponent n for all methods. In particular, the average localization error of the range-based method increased significantly when $n \geq 1.4$. When n was changed from 1.2 to 1.8, the average localization error of the fingerprinting method increased by 3.5 times, while those of proposed method 1 and proposed method 2 increased by 1.4 times and 2.0 times, respectively. We confirmed that the proposed methods using only contact information are robust against environmental changes.

In the proposed methods, the server recognizes the proximity relation between nodes from the RSSI and RSSI threshold R_{th}; thus, the server can dynamically determine R_{th} such that 20% of node pairs are considered to be in proximity. If such dynamical adjustment of the RSSI threshold is applied, the localization accuracy of the proposed methods will be improved.

VI. CONCLUSIONS

Recently, indoor localization based on "proximity/non-proximity" binary values has been studied. The binary value is also employed as contact information in COVID-19 digital contact tracing applications.

In this paper, we have attempted to demonstrate the effectiveness of using only binary contact information. The results of a localization experiment conducted using real devices and those of simulation experiments have shown that the sensor response-based localization method can be applied to indoor localization tasks. Through the simulation experiments, we found that the proposed methods can obtain comparable

accuracy to the existing methods when the attenuation model is accurate. In addition, we have confirmed that the proposed methods, which only consider contact information, are robust against environmental changes even when the attenuation model is inaccurate.

We consider that these contributions have added a new perspective on the use of contact information in the field of indoor localization, which aims to realize power-saving and cost reduction. The simulation results show that setting an optimal RSSI threshold value is required to improve localization accuracy. Thus, in the future, we plan to devise an algorithm to dynamically determine an effective RSSI threshold to realize an optimal rate of proximity nodes.

APPENDIX

A. FORMULATION FOR OPTIMIZATION PROBLEMS

Here, we present the formulation of the optimization problem and the solution of the cooperative localization in Section III-D. We define the observation area as a two-dimensional field with $N(N = |\mathcal{N}|)$ pedestrians. Let $\boldsymbol{a}_i$ denote the known coordinates of anchor node i, and the distance between nodes i and j is expressed as d_{ij}.

The function $g(\boldsymbol{x}_1, \ldots, \boldsymbol{x}_N)$ is defined as follows.

$$g(\boldsymbol{x}_1, \ldots, \boldsymbol{x}_N) \stackrel{\text{def}}{=} \frac{1}{2} \sum_{i \in \mathcal{N}} \sum_{j \in \mathcal{N}_i} (|\boldsymbol{x}_i - \boldsymbol{x}_j| - d_{ij})^2 + \sum_{i \in \mathcal{N}} \sum_{j \in \mathcal{A}_i} (|\boldsymbol{x}_i - \boldsymbol{a}_j| - d_{ij})^2 \quad (15)$$

Here, $g(\boldsymbol{x}_1, \ldots, \boldsymbol{x}_N)$ is minimized by $\boldsymbol{x}_1^{min}, \ldots, \boldsymbol{x}_N^{min}$. In other words, if

$$\forall \boldsymbol{x}_1, \ldots, \boldsymbol{x}_N, \quad g(\boldsymbol{x}_1^{min}, \ldots, \boldsymbol{x}_N^{min}) \leq g(\boldsymbol{x}_1, \ldots, \boldsymbol{x}_N)$$

holds, we consider $\boldsymbol{x}_1^{min}, \ldots, \boldsymbol{x}_N^{min}$ to be the estimated position of the pedestrians calculated from distance d_{ij}. The estimation of $\boldsymbol{x}_1^{min}, \ldots, \boldsymbol{x}_N^{min}$ is discussed in the following.

B. SOLVING THE OPTIMIZATION PROBLEM

Function $g(\boldsymbol{x}_1, \ldots, \boldsymbol{x}_N)$ is a nonconvex nonlinear function, and the global minimum value cannot be obtained analytically; thus, one of the local minimum values obtained by the descent method is employed as the estimated position $\boldsymbol{x}_1, \ldots, \boldsymbol{x}_N$. Here, we introduce an efficient solution to find the local minimum value recursively. First, note that any $\boldsymbol{v}_i$ and $\boldsymbol{v}_j$ have the following relationship:

$$\begin{aligned}
&(|\boldsymbol{x}_i - \boldsymbol{x}_j| - d_{ij})^2 \\
&\quad = |\boldsymbol{x}_i - \boldsymbol{x}_j|^2 + d_{ij}^2 - 2|\boldsymbol{x}_i - \boldsymbol{x}_j| d_{ij} \\
&\quad \leq |\boldsymbol{x}_i - \boldsymbol{x}_j|^2 + d_{ij}^2 - 2(\boldsymbol{x}_i - \boldsymbol{x}_j)(\boldsymbol{v}_i - \boldsymbol{v}_j)^\top \frac{d_{ij}}{|\boldsymbol{v}_i - \boldsymbol{v}_j|} \quad (16)
\end{aligned}$$

The function $s(\boldsymbol{x}_1, \ldots, \boldsymbol{x}_N; \boldsymbol{v}_1, \ldots, \boldsymbol{v}_N)$ is defined as follows:

$$\begin{aligned}
&s(\boldsymbol{x}_1, \ldots, \boldsymbol{x}_N; \boldsymbol{v}_1, \ldots, \boldsymbol{v}_N) \\
&\stackrel{\text{def}}{=} \sum_{i \in \mathcal{N}} \sum_{j \in \mathcal{N}_i} \left\{ |\boldsymbol{x}_i - \boldsymbol{x}_j|^2 + d_{ij}^2 - \frac{2d_{ij}(\boldsymbol{x}_i - \boldsymbol{x}_j)(\boldsymbol{v}_i - \boldsymbol{v}_j)^\top}{|\boldsymbol{v}_i - \boldsymbol{v}_j|} \right\} \\
&\quad + \sum_{i \in \mathcal{N}} \sum_{j \in \mathcal{A}_i} \left\{ |\boldsymbol{x}_i - \boldsymbol{a}_j|^2 + d_{ij}^2 - \frac{2d_{ij}(\boldsymbol{x}_i - \boldsymbol{a}_j)(\boldsymbol{v}_i - \boldsymbol{a}_j)^\top}{|\boldsymbol{v}_i - \boldsymbol{a}_j|} \right\}.
\end{aligned}$$

Note that $g(\boldsymbol{x}_1, \ldots, \boldsymbol{x}_N) = s(\boldsymbol{x}_1, \ldots, \boldsymbol{x}_N; \boldsymbol{x}_1, \ldots, \boldsymbol{x}_N)$. In addition,

$$g(\boldsymbol{x}_1, \ldots, \boldsymbol{x}_N) \leq s(\boldsymbol{x}_1, \ldots, \boldsymbol{x}_N; \boldsymbol{v}_1, \ldots, \boldsymbol{v}_N)$$

holds from (16). Assume that $g(\boldsymbol{x}_1, \ldots, \boldsymbol{x}_N; \boldsymbol{v}_1, \ldots, \boldsymbol{v}_N)$ is minimized at $\boldsymbol{x}_1^{min}, \ldots, \boldsymbol{x}_N^{min}$ for the given $\boldsymbol{v}_1, \ldots, \boldsymbol{v}_N$. In other words,

$$s(\boldsymbol{x}_1^{min}, \ldots, \boldsymbol{x}_N^{m}; \boldsymbol{v}_1, \ldots, \boldsymbol{v}_N) \leq s(\boldsymbol{x}_1, \ldots, \boldsymbol{x}_N; \boldsymbol{v}_1, \ldots, \boldsymbol{v}_N)$$

holds for any $\boldsymbol{x}_1, \ldots, \boldsymbol{x}_N$. Then, we obtain the following:

$$\begin{aligned}
g(\boldsymbol{x}_1^{min}, \ldots, \boldsymbol{x}_N^{min}) &\leq s(\boldsymbol{x}_1^{min}, \ldots, \boldsymbol{x}_N^{min}; \boldsymbol{v}_1, \ldots, \boldsymbol{v}_N) \\
&\leq s(\boldsymbol{v}_1, \ldots, \boldsymbol{v}_N; \boldsymbol{v}_1, \ldots, \boldsymbol{v}_N) \\
&= g(\boldsymbol{v}_1, \ldots, \boldsymbol{v}_N). \quad (17)
\end{aligned}$$

From the above, the local minimum value of the function $g(\boldsymbol{x}_1, \ldots, \boldsymbol{x}_N)$ can be obtained recursively as follows. First, we set the initial solution $\boldsymbol{x}_1^{(1)}, \ldots, \boldsymbol{x}_N^{(1)}$. We then find $\boldsymbol{x}_1, \ldots, \boldsymbol{x}_N$, which minimizes $s(\boldsymbol{x}_1, \ldots, \boldsymbol{x}_N; \boldsymbol{x}_1^{(1)}, \ldots, \boldsymbol{x}_N^{(1)})$, and let it be the second solution $\boldsymbol{x}_1^{(2)}, \ldots, \boldsymbol{x}_N^{(2)}$. Using this procedure, we obtain $\boldsymbol{x}_1^{(k)}, \ldots, \boldsymbol{x}_N^{(k)} (k = 1, 2, \ldots)$ recursively. When $g_k \stackrel{\text{def}}{=} g(\boldsymbol{x}_1^{(k)}, \ldots, \boldsymbol{x}_N^{(k)})$ is defined, $g_1, g_2, \ldots$ becomes a decreasing sequence by (17), and $g(\boldsymbol{x}_1^{(k)}, \ldots, \boldsymbol{x}_N^{(k)})$ converges to the local minimum value of $g(\boldsymbol{x}_1, \ldots, \boldsymbol{x}_N)$ at the limit of $k \to \infty$. Note that the convergence destination is not necessarily the global minimum value of function g.

C. MINIMUM VALUE OF FUNCTION S

In the above procedure, we must find $\boldsymbol{x}_1^{min}, \ldots, \boldsymbol{x}_N^{min}$ that minimizes $s(\boldsymbol{x}_1, \ldots, \boldsymbol{x}_N; \boldsymbol{v}_1, \ldots, \boldsymbol{v}_N)$ for a given $\boldsymbol{v}_1, \ldots, \boldsymbol{v}_N$, and this method is explained as follows. Here, function $s(\boldsymbol{x}_1, \ldots, \boldsymbol{x}_N; \boldsymbol{v}_1, \ldots, \boldsymbol{v}_N)$ is decomposed as follows:

$$\begin{aligned}
&s(\boldsymbol{x}_1, \ldots, \boldsymbol{x}_n; \boldsymbol{v}_1, \ldots, \boldsymbol{v}_N) \\
&\quad = s_1(\boldsymbol{x}_1, \ldots, \boldsymbol{x}_N; \boldsymbol{v}_1, \ldots, \boldsymbol{v}_N) + s_2(\boldsymbol{x}_1, \ldots, \boldsymbol{x}_N; \boldsymbol{v}_1, \ldots, \boldsymbol{v}_N), \\
&s_1(\boldsymbol{x}_1, \ldots, \boldsymbol{x}_N; \boldsymbol{v}_1, \ldots, \boldsymbol{v}_N) \\
&\stackrel{\text{def}}{=} \sum_{i \in \mathcal{N}} \sum_{j \in \mathcal{N}_i} \left\{ |\boldsymbol{x}_i - \boldsymbol{x}_j|^2 + d_{ij}^2 - \frac{2d_{ij}(\boldsymbol{x}_i - \boldsymbol{x}_j)(\boldsymbol{v}_i - \boldsymbol{v}_j)^\top}{|\boldsymbol{v}_i - \boldsymbol{v}_j|} \right\}, \\
&s_2(\boldsymbol{x}_1, \ldots, \boldsymbol{x}_N; \boldsymbol{v}_1, \ldots, \boldsymbol{v}_N) \\
&\stackrel{\text{def}}{=} \sum_{i \in \mathcal{N}} \sum_{j \in \mathcal{A}_i} \left\{ |\boldsymbol{x}_i - \boldsymbol{a}_j|^2 + d_{ij}^2 - \frac{2d_{ij}(\boldsymbol{x}_i - \boldsymbol{a}_j)(\boldsymbol{v}_i - \boldsymbol{a}_j)^\top}{|\boldsymbol{v}_i - \boldsymbol{a}_j|} \right\}.
\end{aligned}$$

Here, $s(\boldsymbol{x}_1, \ldots, \boldsymbol{x}_N; \boldsymbol{v}_1, \ldots, \boldsymbol{v}_N)$ is minimized by $\boldsymbol{x}_1^{min}, \ldots, \boldsymbol{x}_N^{min}$; thus, we obtain

$$\frac{\partial s(\boldsymbol{x}_1, \ldots, \boldsymbol{x}_N; \boldsymbol{v}_1, \ldots, \boldsymbol{v}_N)}{\partial \boldsymbol{x}_i}\bigg|_{\boldsymbol{x}_i = \boldsymbol{x}_i^{min}} = \boldsymbol{0} \tag{18}$$

for all $i \in \mathcal{N}$. In addition,

$$\frac{\partial s_1(\boldsymbol{x}_1, \ldots, \boldsymbol{x}_N; \boldsymbol{v}_1, \ldots, \boldsymbol{v}_N)}{\partial \boldsymbol{x}_i} = \sum_{j \in \mathcal{N}_i} \left\{ (\boldsymbol{x}_i - \boldsymbol{x}_j) - \frac{d_{ij}(\boldsymbol{v}_i - \boldsymbol{v}_j)}{|\boldsymbol{v}_i - \boldsymbol{v}_j|} \right\}, \tag{19}$$

for all $i \in \mathcal{N}$, and

$$\frac{\partial s_2(\boldsymbol{x}_1, \ldots, \boldsymbol{x}_n; \boldsymbol{v}_1, \ldots, \boldsymbol{v}_N)}{\partial \boldsymbol{x}_i} = \sum_{j \in \mathcal{A}_i} \left\{ (\boldsymbol{x}_i - \boldsymbol{a}_j) - \frac{d_{ij}(\boldsymbol{v}_i - \boldsymbol{a}_j)}{|\boldsymbol{v}_i - \boldsymbol{a}_j|} \right\}. \tag{20}$$

We substitute (19) and (20) into (18).

$$\boldsymbol{\beta}_i = (|\mathcal{N}_i + \mathcal{A}_i|)\boldsymbol{x}_i^{min} - \sum_{j \in \mathcal{N}_i} \boldsymbol{x}_j^{min}, \quad i \in \mathcal{N}, \tag{21}$$

$$\boldsymbol{\beta}_i \stackrel{\text{def}}{=} \sum_{j \in \mathcal{N}_i} \frac{d_{ij}(\boldsymbol{v}_i - \boldsymbol{v}_j)}{|\boldsymbol{v}_i - \boldsymbol{v}_j|} + \sum_{j \in \mathcal{A}_i} \frac{d_{ij}(\boldsymbol{v}_i - \boldsymbol{a}_j)}{|\boldsymbol{v}_i - \boldsymbol{a}_j|} + \sum_{j \in \mathcal{A}_i} \boldsymbol{a}_j.$$

Note that (21) are simultaneous linear equations for $\boldsymbol{x}_1^{min}, \ldots, \boldsymbol{x}_N^{min}$; thus, $\boldsymbol{x}_1^{min}, \ldots, \boldsymbol{x}_N^{min}$ can be calculated by solving the simultaneous equations. For example, we define a vector $\boldsymbol{X}_r \stackrel{\text{def}}{=} (x_{x,1}, \ldots, x_{x,N})^\top$ with the x components of $\boldsymbol{x}_1^{min}, \ldots, \boldsymbol{x}_N^{min}$ and vector $\boldsymbol{X}_\beta \stackrel{\text{def}}{=} (\beta_{x,1}, \ldots, \beta_{x,N})^\top$ with the x components of $\boldsymbol{\beta}_1, \ldots, \boldsymbol{\beta}_N$,

$$\boldsymbol{X}_\beta = B\boldsymbol{X}_r,$$

where

$$B \stackrel{\text{def}}{=} \begin{pmatrix} |\mathcal{N}_1 + \mathcal{A}_1| & -A_{12} & \ldots & -A_{1N} \\ -A_{21} & |\mathcal{N}_2 + \mathcal{A}_2| & \ldots & -A_{2N} \\ \vdots & \vdots & \ddots & \vdots \\ -A_{N1} & -A_{N2} & \ldots & |\mathcal{N}_N + \mathcal{A}_N| \end{pmatrix},$$

$$A_{ij} \stackrel{\text{def}}{=} \begin{cases} 0, & j \notin \mathcal{N}_i \\ 1, & j \in \mathcal{N}_i. \end{cases}$$

Here, B has an inverse matrix; thus, $\boldsymbol{X}_r = B^{-1}\boldsymbol{X}_\beta$ holds. Similarly, $(x_{y,1}, \ldots, x_{y,N})^\top = B^{-1}(\beta_{y,1}, \ldots, \beta_{y,N})^\top$. In the above procedure, $\boldsymbol{v}_1, \ldots, \boldsymbol{v}_N$ corresponds to the k-th solution, and $\boldsymbol{x}_1^{min}, \ldots, \boldsymbol{x}_N^{min}$ corresponds to the $(k+1)$-th solution. Note that these change with each recursive calculation; however, B is invariant, and the inverse matrix of B only needs to be calculated once.

REFERENCES

[1] F. Zafari, A. Gkelias, and K. K. Leung, "A survey of indoor localization systems and technologies," *IEEE Commun. Surv. & Tut.*, vol. 21, no. 3, pp. 2568–2599, 2019.

[2] M. Fazio, A. Buzachis, A. Galletta, A. Celesti, and M. Villari, "A proximity-based indoor navigation system tackling the covid-19 social distancing measures," in *2020 IEEE Symp. Comput. Commun.(ISCC)*, IEEE, 2020, pp. 1–6.

[3] Y. Zhao, F. Yin, F. Gunnarsson, M. Amirijoo, E. Özkan, and F. Gustafsson, "Particle filtering for positioning based on proximity reports," in *2015 18th Int. Conf. Infor. Fusion (Fusion)*, IEEE, 2015, pp. 1046–1052.

[4] F. Yin, Y. Zhao, and F. Gunnarsson, "Proximity report triggering threshold optimization for network-based indoor positioning," in *2015 18th Int. Conf. Infor. Fusion (Fusion)*, IEEE, 2015, pp. 1061–1069.

[5] Y. Zhao, C. Fritsche, F. Yin, and F. Gustafsson. "Sequential monte carlo methods and theoretical bounds for proximity report based indoor positioning," *IEEE Trans. Vehicular Tech.*, vol. 67, no. 6, pp. 5372–5386, 2018.

[6] T. Martin, G. Karopoulos, J. L. Hernández-Ramos, G. Kambourakis, and I. N. Fovino, "Demystifying covid-19 digital contact tracing: A survey on frameworks and mobile apps," *Wirel. Commun. Mobile Comput.*, vol. 2020, 2020.

[7] C. Gentner, D. Günther and P. H. Kindt, "Identifying the BLE advertising channel for reliable distance estimation on smartphones" *IEEE Access*, vol. 10, pp. 9563–9575, 2022.

[8] P. H. Kindt, T. Chakraborty, and S. Chakraborty. "How reliable is smartphone-based electronic contact tracing for covid-19?," *Commun. ACM*, vol. 65, no. 1, pp. 56–67, 2021.

[9] S. Shiraki, A. Suzuki, T. Uehara, Y. Ohashi, S. Shioda, "Indoor pedestrian localization methods using contact information from bluetooth low energy beacons between smartphones," in *95th Vehicular Tech. Conf.(VTC2022-Spring)*, IEEE, 2022, pp. 1–7.

[10] S. Shioda, "Localizing sensors from their responses to targets," *IEICE Trans. Commun.*, vol. 98, no. 1, pp. 145–152, 2015.

[11] S. Shiraki, Y. Ohashi, T. Uehara, and S. Shioda, "Verification of error-increasing factors by sensor response-based localization technology through real device experiments," *IEEE Access*, vol. 9, pp. 101729–101740, 2021.

[12] P. Davidson and R. Piché, "A survey of selected indoor positioning methods for smartphones," *IEEE Commun. Surv. & Tut.*, vol. 19, no. 2, pp. 1347–1370, 2016.

[13] S. Subedi and J. Y. Pyun, "A survey of smartphone-based indoor positioning system using rf-based wireless technologies," *Sensors*, vol. 20, no. 24, p. 7230, 2020.

[14] P. Spachos and K. N. Plataniotis, "Ble beacons for indoor positioning at an interactive iot-based smart museum," *IEEE Syst. J.*, vol. 14, no. 3, pp. 3483–3493, 2020.

[15] T. Wu, H. Xia, S. Liu, and Y. Qiao, "Probability-based indoor positioning algorithm using ibeacons," *Sensors*, vol. 19, no. 23, p. 5226, 2019.

[16] W. Xue, W. Qiu, X. Hua, and K. Yu, "Improved Wi-Fi rssi measurement for indoor localization," *IEEE Sensors J.*, vol. 17, no. 7, pp. 2224–2230, 2017.

[17] B. Huang, J. Liu, and W. Sun and F. Yang, "A robust indoor positioning method based on bluetooth low energy with separate channel information," *Sensors*, vol. 19, no. 16, p. 3487, 2019.

[18] R. Faragher and R. Harle, "Location fingerprinting with bluetooth low energy beacons," *IEEE J. Selected Areas in Commun.*, vol. 33, no. 11, pp. 2418–2428, 2015.

[19] Y. C. Pu, and P. C. You, "Indoor positioning system based on BLE location fingerprinting with classification approach," *Appl. Math. Model.*, vol. 62, pp. 654–663, 2018.

[20] L. Bai, F. Ciravegna, R. Bond, and M. Mulvenna, "A low cost indoor positioning system using bluetooth low energy," *IEEE Access*, vol. 8, pp. 136858-136871, 2020.

[21] Apple, "iBeacon." Accessed on June 16, 2022. [Online.] Available:https://developer.apple.com/ibeacon/

[22] S. T. Kouyoumdjieva and G. Karlsson, "Experimental evaluation of precision of a proximity-based indoor positioning system," in *15th Annu. Conf. Wirel. On-demand Netw. Syst. Services (WONS)*, 2019, IEEE, pp. 130–137.

[23] P. Dickinson, G. Cielniak, O. Szymanezyk, and M. Mannion, "Indoor positioning of shoppers using a network of bluetooth low energy beacons," in *Int. Conf. Indoor Positioning and Indoor Navigation (IPIN)*, IEEE, 2016, pp. 1–8.

[24] R. Momose, T. Nitta, M. Yanagisawa, and N. Togawa, "An accurate indoor positioning algorithm using particle filter based on the proximity of bluetooth beacons," in *IEEE 6th Global Conf. Cons. Electronics (GCCE)*, IEEE, 2017, pp. 1–5.

[25] P. C. Ng, J. She, and R. Ran, "A compressive sensing approach to detect the proximity between smartphones and ble beacons," *IEEE IoT J.*, vol. 6, no. 4, pp. 7162–7174, 2019.

[26] Z. D. Tekler, R. Low, B. Gunay, R. K. Andersen, and L. Blessing, "A scalable bluetooth low energy approach to identify occupancy patterns and profiles in office spaces," *Build. Environ.*, vol. 171, p. 106681, 2020.

[27] D. Surian, V. Kim, R. Menon, A. G. Dunn, V. Sintchenko, and E. Coiera, "Tracking a moving user in indoor environments using bluetooth low energy beacons," *J. Biomed. Inform.*, vol. 98, p. 103288, 2019.
[28] S. Lederer, Y. Wang, and J. Gao, "Connectivity-based localization of large-scale sensor networks with complex shape," *ACM Trans. Sensor Netw. (TOSN)*, vol. 5, no. 4, pp. 1–32, 2009.
[29] Y. Shang, W. Ruml, Y. Zhang, and M. P. J. Fromherz, "Localization from mere connectivity," in *4th ACM Int. Symp. Mobile ad hoc Netw. & Comput.*, 2003, pp. 201–212.
[30] N. Patwari, J. N. Ash, S. Kyperountas, A. O. Hero, R. L. Moses, and N. S. Correal, "Locating the nodes: cooperative localization in wireless sensor networks," *IEEE Signal Process. Mag.*, vol. 22, no. 4, pp. 54–69, 2005.
[31] H. Wymeersch, J. Lien and M. Z. Win, "Cooperative localization in wireless networks," *Proc. IEEE*, vol. 97, no. 2, pp. 427–450, 2009.
[32] D. Niculescu and B. Nath, "Dv based positioning in ad hoc networks," *Telecommun. Syst.*, vol. 22, no. 1, pp. 267–280, 2003.
[33] E. R. Gansner, Y. Koren, and S. North, "Graph drawing by stress majorization," in *Int. Symp. Graph Drawing*, Springer, 2005, pp. 239–250.
[34] Raspberry Pi, "Buy a Raspberry Pi 4 Model B." Accessed on June 16, 2022. [Online.] Available:https://www.raspberrypi.com/products/raspberry-pi-4-model-b/
[35] D. Helbing and P. Molnar, "Social force model for pedestrian dynamics," *Physical review E*, vol. 51, no. 5, p. 4282, 1995.
[36] D. Helbing, I. Farkas, and T. Vicsek, "Simulating dynamical features of escape panic," *Nature*, vol. 407, no. 6803, pp. 487–490, 2000.

SHINO SHIRAKI (Member, IEEE) received her B.E. and M.E. degrees in Urban Environment Systems Engineering from Chiba University, Japan, in 2019 and 2021, respectively. Her research interests include wireless sensor networks, IoT, and indoor localization. She is a member of IEEE and IEICE.

SHIGEO SHIODA (Member, IEEE) received his B.S. degree in Physics from Waseda University in 1986, his M.S. degree in Physics from the University of Tokyo in 1988, and his Ph.D. degree in Teletraffic Engineering from the University of Tokyo, Japan, in 1998. In 1988, he joined Nippon Telegraph and Telephone Corporation, where he was engaged in research on traffic measurements and controls for ATM-based networks. He moved to Chiba University in 2001. Currently, he is a professor in the Department of Architecture and Urban Science, Graduate School of Engineering, Chiba University, Japan. His current research interests include wireless sensor networks, wireless LANs, peer-to-peer systems, and online social networks. He received the Network System Research Award, Information Network Research Award, and Communications Society Distinguished Contributions Award of IEICE in 2003, 2004, 2007, and 2013, respectively, and the IEEE MASS Best Poster Award in 2013. He is a member of ACM, IEEE, and the Operation Research Society of Japan.